Computers and Structures 88 (2010) 483–496

Contents lists available at ScienceDirect

Computers and Structures

journal homepage: www.elsevier.com/locate/compstruc

Hierarchical semi-active control of base-isolated structures using a new inverse model of magnetorheological dampers ☆

Arash Bahar [a], Francesc Pozo [b,*], Leonardo Acho [b], José Rodellar [a], Alex Barbat [c]

[a] CoDAlab, Departament de Matemàtica Aplicada III, Escola Tècnica Superior d'Enginyers de Camins, Canals i Ports de Barcelona (ETSECCPB), Universitat Politècnica de Catalunya (UPC), Jordi Girona, 1-3, 08034 Barcelona, Spain
[b] CoDAlab, Departament de Matemàtica Aplicada III, Escola Universitària d'Enginyeria Tècnica Industrial de Barcelona (EUETIB), Universitat Politècnica de Catalunya (UPC), Comte d'Urgell, 187, 08036 Barcelona, Spain
[c] CIMNE, Departament de Resistència de Materials i Estructures a l'Enginyeria, Escola Tècnica Superior d'Enginyers de Camins, Canals i Ports de Barcelona (ETSECCPB), Universitat Politècnica de Catalunya (UPC), Jordi Girona, 1-3, 08034 Barcelona, Spain

ARTICLE INFO

Article history:
Received 12 March 2009
Accepted 7 January 2010
Available online 10 February 2010

Keywords:
MR damper
Parameter identification
Benchmark building

ABSTRACT

Magnetorheological (MR) dampers have received special attention as semi-active devices for mitigation of structural vibrations. Because of the inherent nonlinearity of these devices, it is difficult to obtain a reasonable mathematical inverse model. This paper is concerned with two related concepts. On one hand, it presents a new inverse model of MR dampers based on the normalized Bouc–Wen model. On the other hand, it considers a hybrid seismic control system for building structures, which combines a class of passive nonlinear base isolator with a semi-active control system. In this application, the MR damper is used as a semi-active device in which the voltage is updated by a feedback control loop. The management of MR dampers is performed in a hierarchical way according to the desired control force, the actual force of the dampers and its capacity to react. The control is applied to a numerical three-dimensional benchmark problem which is used by the structural control community as a state-of-the-art model for numerical experiments of seismic control attenuation. The performance indices show that the proposed semi-active controller behaves satisfactorily.

1. Introduction

Base isolation is one of the most well accepted methods to protect moderate hight and weight structures from earthquake hazard because of its simplicity, reliability, and effectiveness [17]. This system by itself can reduce the interstory drift and the absolute acceleration of the structure, but the absolute base displacement of the structure may be large and hard to accommodate. Passive high-damping devices incorporated within the isolation system can control large bearing displacements associated with pulse-like earthquake ground motions, but the beneficial effects of the base isolation system may be significantly reduced for both moderate and strong earthquakes due to the transfer of energy into higher modes which can result in increased interstory drift and floor acceleration responses [10,14]. Semi-active controllers in hybrid base-isolation systems can achieve almost the same performance as an active base isolation system in protecting the safety of buildings against strong earthquakes [8]. Therefore, a hybrid base isolation system with semi-active devices, like MR dampers, in parallel to isolation bearings, can significantly overcome this problem by means of the application of a single force at the base [14].

A variety of semi-active control algorithms have been proposed for control of MR dampers (see for example [7]). However, one of the most important and challenging tasks in control design is the development of an accurate mathematical model of the structural system under consideration. This model must include both the structure and the control devices.

Many works have been done to model the hysteretic behavior of MR dampers statically or dynamically. For example, various modifications on the Bouc–Wen model have been investigated [2,12]. In these models the input–output relation are expressed by a set of nonlinear differential equations. Although the models can simulate the nonlinear behavior of MR dampers, they have complex structures which make the inverse process hard and time consuming. The inverse model of an MR damper is an efficient way to compute the necessary command voltage which has to be applied according to a desired control force.

☆ Supported by CICYT (Spanish Ministry of Science and Innovation) through Grants DPI2008-06463-C02-01 and DPI2008-06564-C02-02.

* Corresponding author.
E-mail addresses: arash.bahar@upc.edu (A. Bahar), francesc.pozo@upc.edu (F. Pozo), leonardo.acho@upc.edu (L. Acho), jose.rodellar@upc.edu (J. Rodellar), alex.barbat@upc.edu (A. Barbat).
URLs: http://www-ma3.upc.es/codalab (F. Pozo), http://www.cimne.upc.es (A. Barbat).

0045-7949/$ - see front matter © 2010 Elsevier Ltd. All rights reserved.
doi:10.1016/j.compstruc.2010.01.006

In this paper we firstly discuss a new inverse model for MR dampers which are represented using the normalized Bouc–Wen model [1,5]. Then, using this inverse model, we consider a hybrid seismic control system for building structures, which combines a set of passive base isolators with a semi-active control system. Because the force generated in the MR dampers is dependent on the local responses of the structural system, the *desired* control force cannot always be produced by the devices. Only the control voltage can be directly controlled to increase or decrease the force produced by the devices. The desired control force is based on an active controller presented in [13] which has shown sufficient compatibility with the inherent characteristics of MR dampers. In general, in the semi-active control strategies presented in the literature, for instance [7], they managed a single MR damper per floor or, in the case of multiple MR dampers, they receive the same command voltage. In this work, a new practical method has also been defined to compute the command voltage of each MR damper independently according to the desired control force. The management of these MR dampers is based on a hierarchical strategy: we first compare the total damping force generated in the MR dampers with respect to the desired control force and then we decide what dampers need to apply more damping force and the corresponding command voltage. The whole method is simulated by considering a three-dimensional smart base-isolated benchmark building [11] where the MR dampers are used as supplemental damping devices. This benchmark problem is a new generation of benchmark studies by the American Society of Civil Engineering (ASCE) Structural Control Committee, that offers a carefully modeled real-world structure in which different control strategies can be implemented and compared.

2. The magnetorheological damper model

Magnetorheological (MR) dampers are devices that employ rheological fluids to modifiy their mechanical properties. In this respect, the characteristics of the MR damper change when the rheological fluid is exposed to a magnetic field changing its stiffness and damping. In this paper, these devices are used as a semi-active actuators in which the voltage is updated by a feedback control loop. However, an accurate mathematical model and the identification of the system under consideration is needed. In this section we present the phenomenological Bouc–Wen model of an MR damper. The MR dampers in the benchmark building are identified using this model.

The normalized version of the Bouc–Wen model [6] is an equivalent representation of the original Bouc–Wen model [18]. Since this representation is not a linear-in-parameter model, classical parameter identification methods cannot be applied. In this regard, a new parameter identification algorithm was proposed in [6, p. 38], which is based on a physical understanding of the device along with a black box description. This methodology was used in [16] for a large-scale MR damper. The method is based on applying a periodic input velocity $\dot{x}(t)$ at a constant voltage coil v and observing the periodic steady-state force response of the MR damper. Nonetheless, large relative errors in the identification process can be observed when the MR damper has a viscous friction small enough with respect to the dry friction. To cope with this drawback, when the displacement is large enough, an alternative method based on the plastic region of the force-velocity diagram of the MR damper was proposed in [15]. However, the model may not give an accurate representation of large-scale MR dampers which do not belong to the shear-type category [1]. To improve the accuracy of the model representation and, consequently, the accuracy of the parameter identification, the following extended Bouc–Wen model was recently proposed by the authors in [1]:

$$\Phi(x,\dot{x},w)(t) = \kappa_x x(t) + \kappa_{\dot{x}}\dot{x}(t) + \kappa_w w(t), \tag{1}$$

$$\dot{w}(t) = \rho\Big(\dot{x}(t) - \sigma|\dot{x}(t)||w(t)|^{n-1}w(t) + (\sigma-1)\dot{x}(t)|w(t)|^{n}\Big), \tag{2}$$

where the term $\kappa_x x(t)$, which represents a linear elastic force, has been added. The coefficient κ_x is voltage-dependent, as the other parameters. The input–output variables of the MR damper are schematized in Fig. 1.

2.1. Identification results

The identification algorithm proposed in [1] is divided in two steps: (a) the estimation of the value of κ_x and (b) the estimation of the rest of the parameters based on the identification algorithm in [16].

More precisely, in order to implement this identification procedure to identify the parameters of the MR dampers in the benchmark building, it is necessary to apply a periodic excitation displacement and observe the corresponding MR damper force. Fig. 2 illustrates these two signals for a zero voltage. A set of experiments have been performed for different voltages in the range $[0,1]$ volts. This is the range we have considered in this paper, but this is not restricted: a more general range $[0, V_{\max}]$ can be also considered.

The resulting values of the parameters of the model in Eqs. (1) and (2) are listed in Table 1. Fig. 3 plots these parameters as a function of the voltage. To find an accurate voltage-dependent relation of these parameters, and according with the functional dependence observed in Fig. 3, it is considered that $\kappa_x(v)$ is constant, $\kappa_{\dot{x}}(v)$ is linear and $n(v), \rho(v)$ and $\sigma(v)$ are exponential:

$$\kappa_x(v) = \kappa_x \tag{3}$$

$$\kappa_{\dot{x}}(v) = \kappa_{\dot{x},a} + \kappa_{\dot{x},b}\, v \tag{4}$$

$$n(v) = n_a + n_b e^{-13v} \tag{5}$$

$$\rho(v) = \rho_a + \rho_b e^{-14v} \tag{6}$$

$$\sigma(v) = \sigma_a + \sigma_b e^{-14v} \tag{7}$$

Because of the importance of the parameter κ_w due to its great influence in the resulting force (the range of its magnitude is, approximately, from 50 kN to 1000 kN, as can be seen in Table 1), its voltage dependence function is estimated in three different regions in the form

$$\kappa_w(v) = \begin{cases} \kappa_{w_1} + \kappa_{w_2}\, v^{1.15}, & v \leqslant 0.3 \\ \kappa_{w_3} + \kappa_{w_4}\sin\left(\frac{\pi(v-0.3)}{0.8}\right) + \kappa_{w_5}\sin\left(\frac{3\pi(v-0.3)}{0.8}\right), & 0.3 \leqslant v \leqslant 0.7, \\ \kappa_{w_6} + \kappa_{w_7}\, v + \kappa_{w_8}\, v^3 + \kappa_{w_9}\, v^5, & 0.7 \leqslant v \end{cases} \tag{8}$$

based on the variation of the resulting values (Fig. 4).

The coefficients $\kappa_{\dot{x},a}, \kappa_{\dot{x},b}, \kappa_{w1}, \ldots, \kappa_{w9}, n_a, n_b, \rho_a, \rho_b, \sigma_a$ and σ_b have been computed using MATLAB. Their values are listed in Table 2. The voltage-dependent functions are plotted in Fig. 3, where a very good matching is observed.

Fig. 1. Input–output variables of the MR damper.

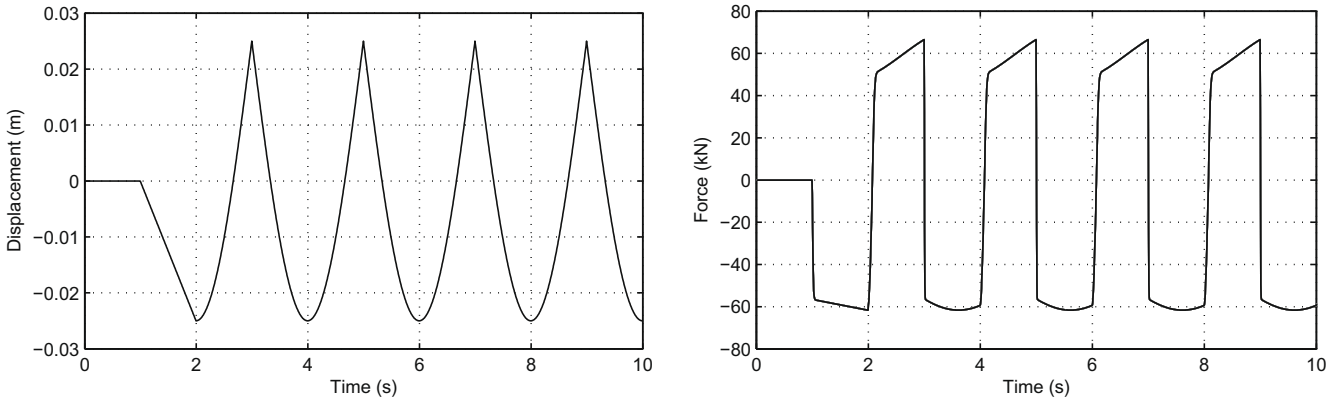

Fig. 2. Response of the MR damper model in the benchmark building platform.

Table 1
Identification results.

v	κ_x	$\kappa_{\dot{x}}$	κ_w	ρ	n	σ
0.00	207	89.643	54.652	644.92	1.4557	0.7733
0.05	207	104.24	125.97	647.34	1.4436	0.7674
0.10	207	118.84	214.49	648.11	1.4398	0.7656
0.15	207	133.44	313.47	648.45	1.4381	0.7648
0.20	207	148.04	416.96	648.64	1.4372	0.7643
0.25	207	162.64	519.87	648.75	1.4366	0.7641
0.30	207	177.24	617.94	648.82	1.4362	0.7639
0.35	207	191.84	707.73	648.87	1.4360	0.7638
0.40	207	206.44	786.63	648.90	1.4358	0.7637
0.45	207	221.04	852.86	648.92	1.4357	0.7636
0.50	207	235.64	905.48	648.94	1.4357	0.7636
0.55	207	205.25	944.37	648.95	1.4356	0.7636
0.60	207	264.84	970.24	648.96	1.4356	0.7636
0.65	207	279.44	984.64	648.96	1.4355	0.7636
0.70	207	294.04	989.94	648.96	1.4355	0.7636
0.75	207	308.64	989.34	648.96	1.4355	0.7636
0.80	207	323.24	986.89	648.96	1.4355	0.7636
0.85	207	337.84	987.43	648.96	1.4355	0.7636
0.90	207	352.44	996.67	648.96	1.4355	0.7638
0.95	207	367.04	1021.1	648.96	1.4355	0.7636
1.00	207	381.64	1068.2	648.98	1.4355	0.7635

3. Hierarchical semi-active control algorithm development

There exists a wide range of control algorithms that are applied to base-isolated buildings: clipped-optimal control [3,7,19]; maximum energy dissipation algorithms [9]; and modulated homogeneous friction algorithms, among others. Each of these controllers is able to reduce the structural response to some degree. From a structural point of view, a reasonable controller has to reduce the base displacement while decreases or slightly increases the accelerations. Li and Ou [8] showed that the active control forces in base-isolated structures have damping characteristics. In addition, an active robust control for nonlinear base-isolated structures which has a damping characteristic and is in line with the results of [8] was proposed in [13]. In this study, this class of active controller will be applied in a semi-active way to the base-isolated benchmark building [11]. The control forces will be applied at the base through manipulation of the command voltage at the MR dampers.

3.1. The desired control force

For control design, a nonlinear base-isolated building structure as shown in Fig. 5 is considered. More precisely, a dynamic model composed of two coupled subsystems, namely, the main structure or superstructure (S_r) and the base isolation (S_c), is employed:

$$S_r : \mathbf{M}\ddot{\mathbf{x}} = -\mathbf{M}\mathbf{J}\ddot{x}_g - \mathbf{C}\dot{\mathbf{r}} - \mathbf{K}\mathbf{r} \tag{9}$$

$$S_c : m\ddot{x} + c\dot{x} + kx = c_1\dot{r}_1 + k_1 r_1 - \Omega(x,t) - m\ddot{x}_g + f \tag{10}$$

where $\ddot{x}_g$ is the absolute ground acceleration, $\mathbf{x} = [x_1, x_2, \ldots, x_8]^{\mathrm{T}} \in \mathbb{R}^8$ represents the horizontal displacements of each floor with respect to the ground and f is a horizontal control force. The mass, damping and stiffness of the ith storey is denoted by m_i, c_i and k_i, respectively, $\mathbf{r} = [r_1, \ldots, r_8]^{\mathrm{T}} \in \mathbb{R}^8$, represents the horizontal displacements of the ith floor relative to the $(i-1)$th floor. The base isolation is described as a single degree of freedom with horizontal displacement x. It is assumed to exhibit a linear behavior characterized by mass, damping and stiffness m, c and k, respectively, plus a nonlinear behavior represented by a restoring force $\Omega(x,t)$. The matrices $\mathbf{M}, \mathbf{C}, \mathbf{K}$ and $\mathbf{J}$ of the structure have the following form:

$$\mathbf{M} = \mathrm{diag}(m_1, m_2, \ldots, m_8) \in \mathbb{R}^{8\times 8}$$

$$\mathbf{J} = [1, \ldots, 1]^{\mathrm{T}} \in \mathbb{R}^8$$

$$\mathbf{C} = (c_{ij}) \in \mathbb{R}^{8\times 8}, \quad c_{ij} = \begin{cases} c_i, & i = j \\ -c_{i+1}, & j - i = 1 \\ 0, & \text{otherwise} \end{cases}$$

$$\mathbf{K} = (k_{ij}) \in \mathbb{R}^{8\times 8}, \quad k_{ij} = \begin{cases} k_i, & i = j \\ -k_{i+1}, & j - i = 1 \\ 0, & \text{otherwise} \end{cases}$$

Assuming that the earthquake disturbance is unknown but bounded, the following velocity feedback control law (desired control force) is considered [13]:

$$f_{\mathrm{d}} = -\varrho\,\mathrm{sgn}(\dot{x}), \tag{11}$$

where ϱ is a positive real number.

3.2. The inverse model

The inverse model will provide a suitable tool to compute the command voltage of MR dampers analytically. Consider again the extended normalized form of the Bouc–Wen model for MR dampers:

$$\Phi(x,\dot{x},w)(t) = \kappa_x(v)x(t) + \kappa_{\dot{x}}(v)\dot{x}(t) + \kappa_w(v)w(t),$$

where $\Phi(x,\dot{x},w)(t)$ is the output force of the MR damper. It has been proved in Section 2 that κ_x is constant, $\kappa_{\dot{x}}(v) = \kappa_{\dot{x},a} + \kappa_{\dot{x},b}v$ is linear and $\kappa_w(v)$ is a piecewise nonlinear function defined in Eq. (8). The inverse model (see Fig. 6), that is, the computation of the voltage v as a function of the displacement, velocity and force, is based on two simplifications:

(a) on one hand, the piecewise nonlinear function κ_w is replaced by a piecewise linear representation as illustrated in Fig. 7:

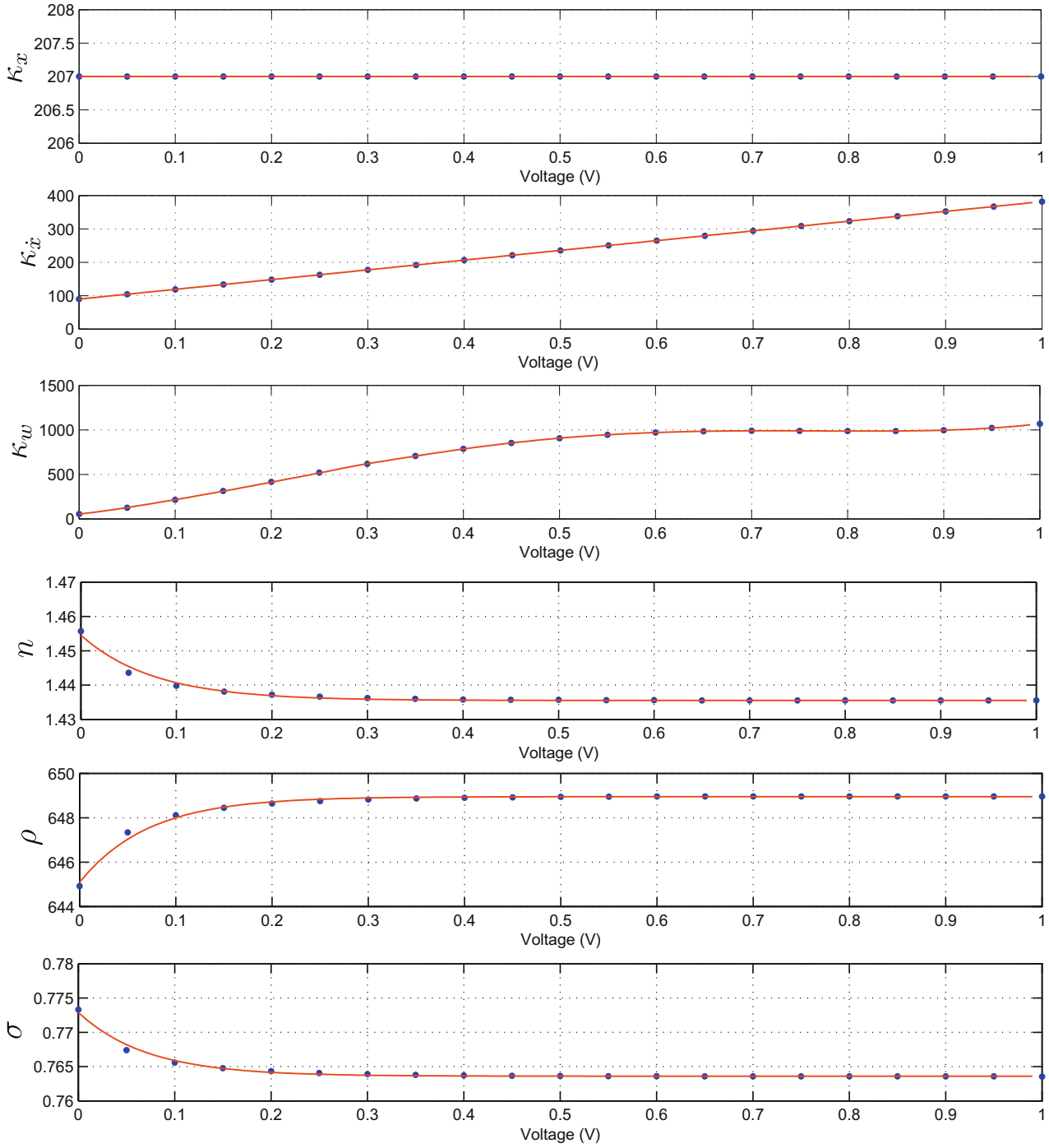

Fig. 3. Results of the parameter identification algorithm (dots) and corresponding model curve fitting (solid).

$$\kappa_w(v) = \kappa_{w,a} + \kappa_{w,b}\, v,$$

where $\kappa_{w,a}$ and $\kappa_{w,b}$ are defined in Table 3;

(b) on the other hand, the internal dynamic variable $w(t)$, which is unmeasurable, is replaced by the sign of the velocity:

$$w(t) = \mathrm{sgn}(\dot{x}) \in \{-1, 1\}.$$

We remark that, in the normalized version of the Bouc–Wen model, the value of this internal dynamic variable lies within the range $[-1, 1]$. The feasibility of this simplification is illustrated in Fig. 8.

As a result of this simplification, the MR damper model is

$$\begin{aligned}\Phi(x, \dot{x}, w)(t) &= \kappa_x x(t) + (\kappa_{\dot{x},a} + \kappa_{\dot{x},b}\, v)\dot{x}(t) + (\kappa_{w,a} + \kappa_{w,b}\, v)\mathrm{sgn}(\dot{x}) \\ &= \kappa_x x(t) + \kappa_{\dot{x},a}\dot{x}(t) + \kappa_{w,a}\mathrm{sgn}(\dot{x}) \\ &\quad + \left(\kappa_{\dot{x},b}\dot{x}(t) + \kappa_{w,b}\mathrm{sgn}(\dot{x})\right) v\end{aligned}$$

Thereby, the final form of the inverse model will be:

$$v(x, \dot{x}, \Phi) = \frac{\Phi - \kappa_x x(t) - \kappa_{\dot{x},a}\dot{x}(t) - \kappa_{w,a}\mathrm{sgn}(\dot{x}(t))}{\kappa_{\dot{x},b}\dot{x}(t) + \kappa_{w,b}\mathrm{sgn}(\dot{x}(t))}. \tag{12}$$

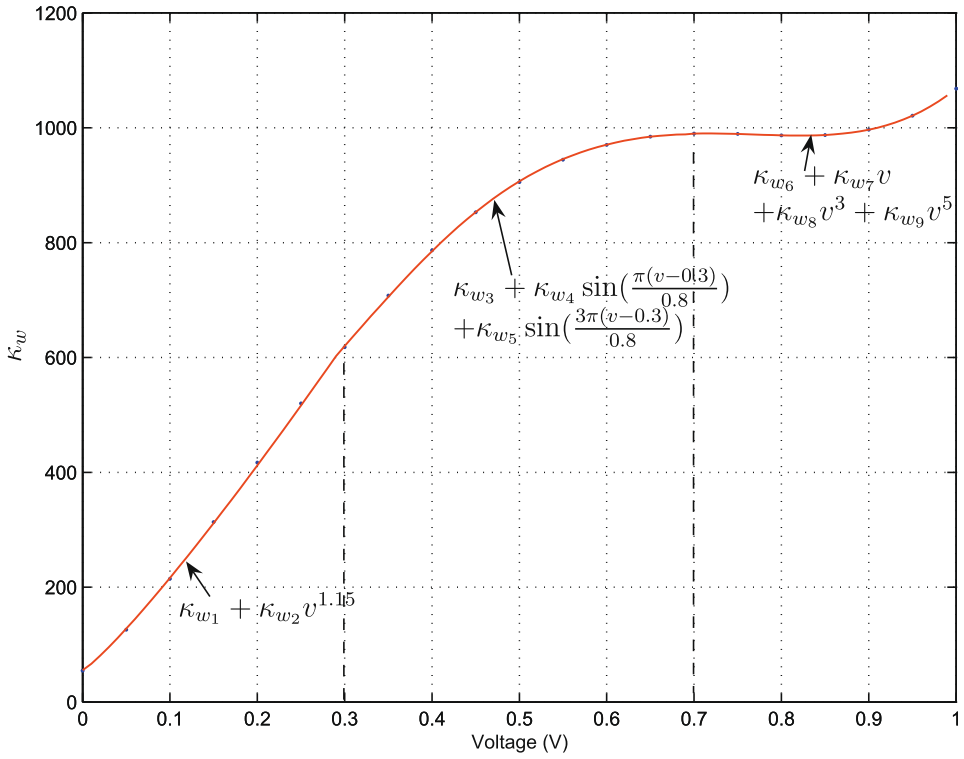

Fig. 4. The voltage dependence of the parameter $\kappa_w(v)$ is estimated in three different regions.

Table 2
Identification results.

Parameter		Value
κ_x		207
$\kappa_{\dot{x}}$	$\kappa_{\dot{x},a}$	89.64
	$\kappa_{\dot{x},b}$	292
ρ	ρ_a	648.95
	ρ_b	-3.86
n	n_a	1.44
	n_b	0.02
σ	σ_a	0.76
	σ_b	0.009
κ_w	κ_{w1}	55.38
	κ_{w2}	2270.0
	κ_{w3}	619.85
	κ_{w4}	387.34
	κ_{w5}	18.42
	κ_{w6}	−87.52
	κ_{w7}	2665.0
	κ_{w8}	−3054.7
	κ_{w9}	1545.5

3.3. The selection of the command voltage v

It is well known that the force generated by the MR damper cannot be commanded; only the voltage v applied to the current driver for the MR damper can be directly changed [3]. In the clipped-optimal control algorithm [3], the command voltage takes the values zero or the maximum, according to

$$v = V_{\max} H\{(f_d - f_{MR}) f_{MR}\},$$

where $V_{\max}$ is the maximum voltage to the current driver associated with saturation of the magnetic field in the MR damper, $H(\cdot)$ is the Heaviside step function, f_d is the desired control force and f_{MR} is the measured force of the MR damper. In some situations, when the

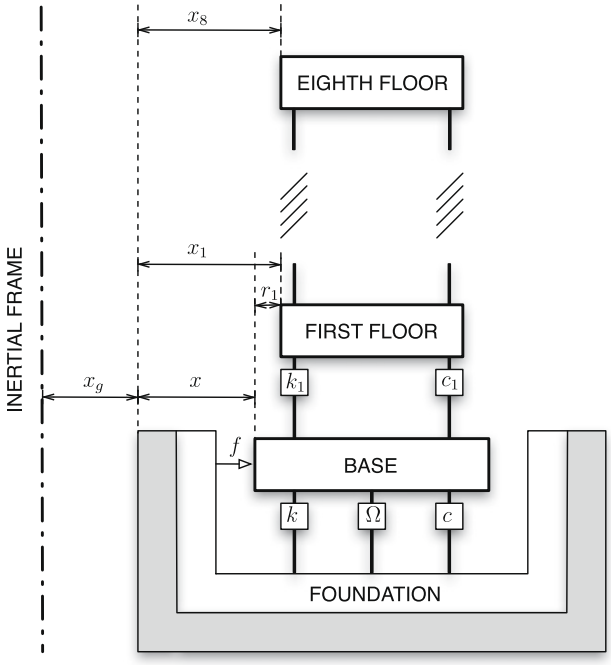

Fig. 5. Base-isolated structure with active control.

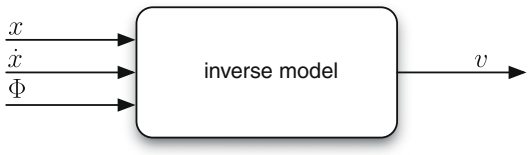

Fig. 6. Input-output variables of the inverse model.

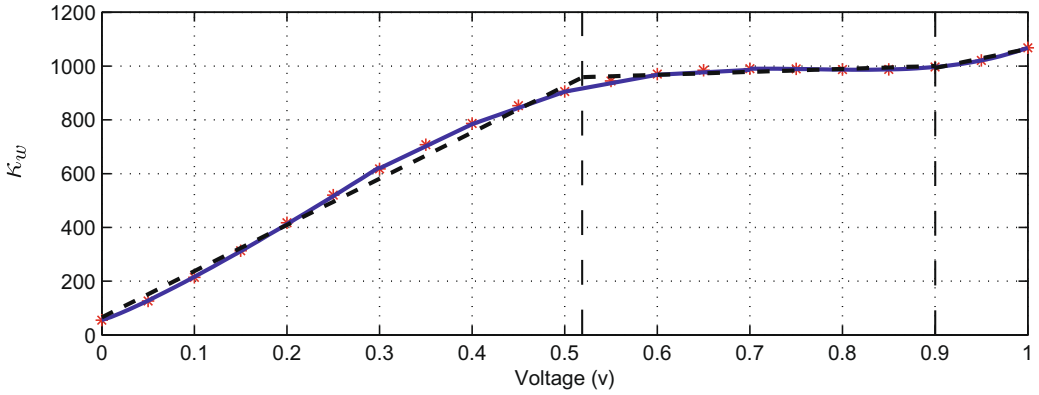

Fig. 7. The piecewise nonlinear function k_w (solid) is approximated by a piecewise linear representation (dashed).

Table 3
Parameters of the inverse model.

Parameter			Value
κ_x			207
$\kappa_{\dot{x}}$	$\kappa_{\dot{x},a}$		89.64
	$\kappa_{\dot{x},b}$		292
κ_w	$\kappa_{w,a}$	$0 \leqslant v < 0.52$	65.2
		$0.52 \leqslant v < 0.9$	902.1
		$0.9 \leqslant v \leqslant 1$	349.1
	$\kappa_{w,b}$	$0 \leqslant v < 0.52$	1720.8
		$0.52 \leqslant v < 0.9$	109.10
		$0.9 \leqslant v \leqslant 1$	715.3

dominant frequencies of the system under control are low, large changes in the forces applied to the structure may result in high local acceleration [19]. In this sense, a modification to the original clipped-optimal control algorithm in which the control voltage can be any value between zero and a $V_{\max}$, was proposed in [19]. A similar approach can be found in [4], where a force-feedback control scheme is employed to overcome the difficulty of commanding the MR damper to produce an arbitrary force. In this paper we consider the same idea of changing the voltage but according to the inverse model in Eq. (12). More precisely, to induce the MR damper to generate approximately the desired control force f_d, the algorithm for selecting the command signal can be concisely stated as

$$v = \frac{f_d - \left(\kappa_x x + \kappa_{\dot{x},a}\dot{x} + \operatorname{sgn}(\dot{x})\kappa_{w,a}\right)}{\kappa_{\dot{x},b}\dot{x} + \operatorname{sgn}(\dot{x})\kappa_{w,b}}, \tag{13}$$

where f_d is computed according to

$$f_d = -\varrho \operatorname{sgn}(\dot{x}). \tag{14}$$

Both Eqs. (13) and (14) define a semi-active controller. Fig. 9 illustrates the corresponding closed-loop system.

3.4. Hierarchical control scheme

In the benchmark building considered in this paper, MR dampers are placed at eight specific locations. At each location, there are two controllers-one in the x- and the other in the y-direction. These actuators are used to apply the damping control forces to the base of the structure.

This section proposes a overall strategy to implement the previous control loop no through a single damper but by means of a set of several MR dampers.

The final goal of the semi-active control scheme is that the total damping force generated by the whole set of MR dampers closely

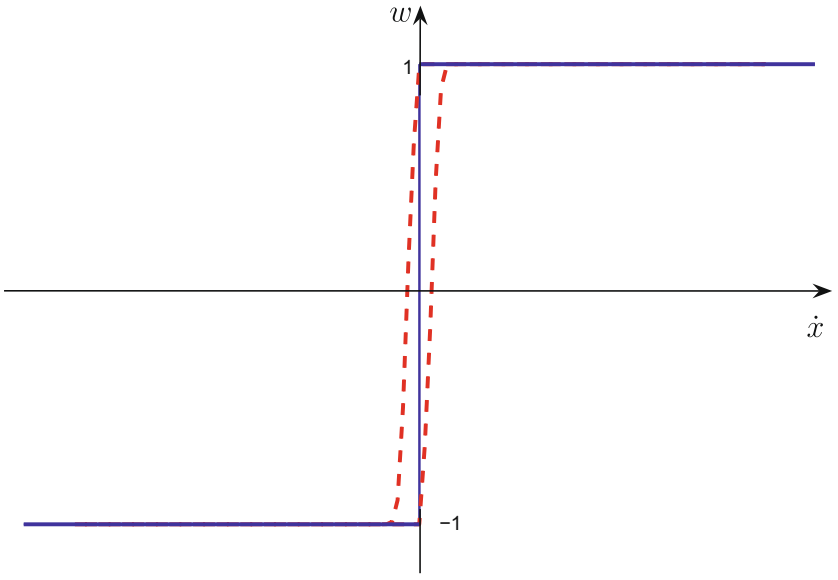

Fig. 8. The internal dynamic variable $w(t)$ is approximated by the sign of the velocity.

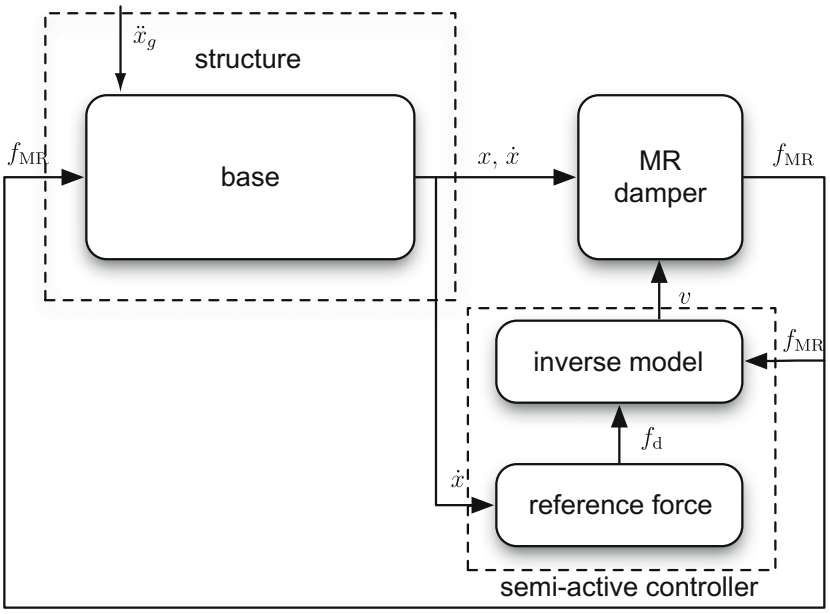

Fig. 9. Block diagram of the semi-active control system for a single MR damper.

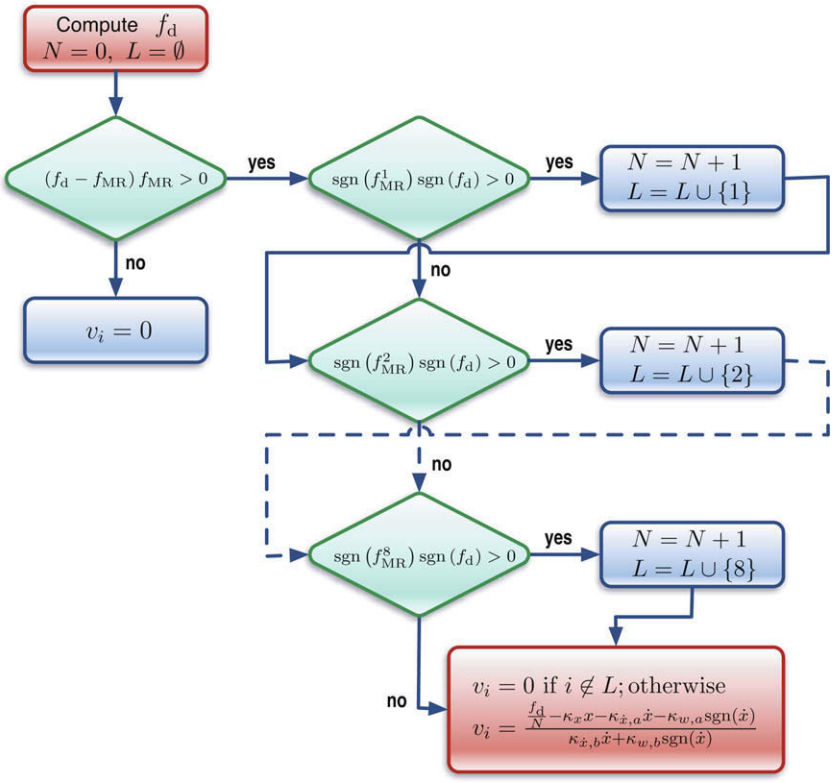

Fig. 10. Hierarchical semi-active control: flow diagram.

follows the desired control force f_{d}. With this aim, we propose a hierarchical semi-active control strategy as illustrated in Fig. 10. With this scheme, we have to decide whether it is necessary to apply voltage to the dampers, to which dampers, and the magnitude of the voltage. More precisely, this procedure can be summarized in the following steps to be implemented real-time at each sampling instant:

Step 1. Compute the desired control force f_{d}, according to the control law in Eq. (14).

Step 2. If the magnitude of the total damping force generated (measured) by the MR dampers, $f_{\mathrm{MR}} := \sum_{i=1}^{8} f^i_{\mathrm{MR}}$, is smaller than the magnitude of the desired control force f_{d} and the two forces have the same sign, that is, if the following expression holds

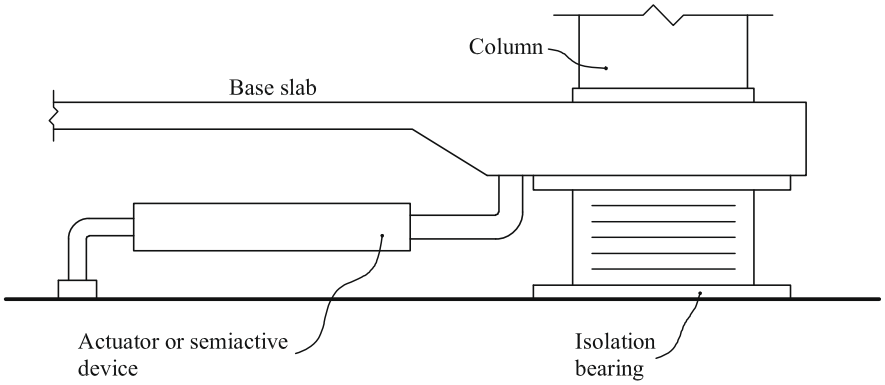

Fig. 11. Elevation view with devices.

$$(f_d - f_{MR})f_{MR} > 0,$$

it means that the MR dampers need to apply more damping force and then we go to `Step 3`. Otherwise, the voltage applied to each damper is set to $v_i = 0,\ i = 1,\ldots,8$, and we leave them work *passively*.

Step 3. Compute the number of dampers that are applying force in the same direction that the desired control force. In this sense, we define the following set

$$L = \{i \in \{1,\ldots 8\} | \mathrm{sgn}(f^i_{MR})\mathrm{sgn}(f_d) > 0\}.$$

Let N be the cardinal of this set.

Step 4. Compute the corresponding command voltage. Each of the N dampers has to offer a part of the control force equal to $\frac{f_d}{N}$. Based on this desired value and Eq. (14), the corresponding command voltage that has to be applied to each damper will be calculated in the form

$$v_i = \frac{\frac{f_d}{N} - \kappa_x x - \kappa_{\dot{x},a}\dot{x} - \kappa_{w,a}\mathrm{sgn}(\dot{x})}{\kappa_{\dot{x},b}\dot{x} + \kappa_{w,b}\mathrm{sgn}(\dot{x})}, \quad i \in L,\ v_i = 0, \quad i \notin L.$$

In the implementation of this formula, the resulting values are truncated between zero and one, that is, if the voltage is negative, the output will be zero; if the voltage is greater than one, the output will be just one. More precisely, the applied voltage v_a will be finally computed as:

$$v_a = \min\{\max\{0, v(x,\dot{x},f_d)\}, 1\}.$$

4. Smart base-isolated benchmark building

The smart base-isolated benchmark building [11] is employed as an interesting and more realistic example to further investigate the effectiveness of the proposed design approach. This benchmark problem is recognized by the American Society of Civil Engineers (ASCE) Structural Control Committee as a state-of-the-art model developed to provide a computational platform for numerical experiments of seismic control attenuation.

The benchmark structure is an eight-storey frame building with steel-braces, 82.4 m long and 54.3 m wide, similar to existing buildings in Los Angeles, California. Stories one to six have an L-shaped plan while the higher floors have a rectangular plan. The superstructure rests on a rigid concrete base, which is isolated from the ground by an isolator layer, and consists of linear beam, column and bracing elements and rigid slabs.

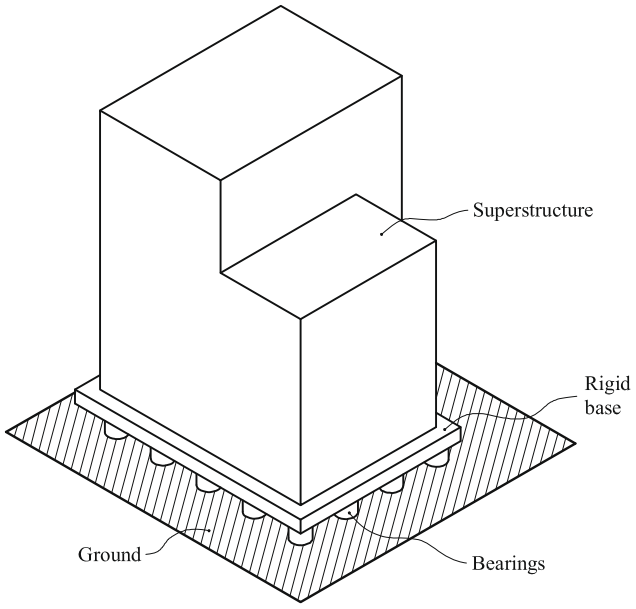

Fig. 12. A representative figure of the benchmark structure.

Below the base, the isolation layer consists of a variety of 92 isolation bearings. The isolators are connected between the drop panels and the footings below, as shown in Fig. 11. See Fig. 12 for a representative figure of the benchmark structure.

5. Numerical results

The performance of the semi-active control algorithm presented in Section 3 is now evaluated through numerical simulation using the smart base-isolated benchmark building. The results of the semi-active control strategy are summarized in Tables 4 and 5, for the fault normal (FN) and the fault parallel (FP) components acting in two perpendicular directions. The results are also compared with the clipped-optimal control algorithm in [3] and also with two limit cases: *passive off* and *passive on*, that corresponds to the cases of *zero* voltage and *maximum* voltage. The evaluation is reported in terms of the performance indices described in the Appendix A. The controlled benchmark structure is simulated for seven earthquake ground accelerations defined in the benchmark problem (Newhall, Sylmar, El Centro, Rinaldi, Kobe, Ji-Ji and Erzinkan). All the excitations are used at the full intensity for the evaluation of the performance indices. The performance

Table 4
Evaluation criteria for the proposed semi-active scheme compared with the clipped-optimal control algorithm in [3] and also with two limit cases: *passive off* and *passive on* (FP-*x* and FN-*y*).

Earthq.	Case	J_1	J_2	J_3	J_4	J_5	J_6	J_7	J_8	J_9
Newhall	P-On	0.91	0.95	0.51	**1.30**	**2.49**	0.34	0.25	**1.07**	0.89
	P-Off	0.93	0.91	0.81	0.94	0.97	0.05	0.71	0.86	0.41
	Clip.	0.97	**1.01**	0.56	**1.03**	**1.48**	0.30	0.33	0.89	0.79
	Prop.	0.83	0.84	0.61	0.94	**1.09**	0.19	0.36	0.69	0.79
Sylmar	P-On	0.90	0.92	0.66	0.81	**1.49**	0.25	0.40	0.82	0.86
	P-Off	0.98	0.97	0.95	0.96	0.99	0.04	0.82	0.91	0.35
	Clip.	0.90	0.91	0.73	0.87	**1.16**	0.24	0.45	0.74	0.81
	Prop.	0.89	0.90	0.78	0.82	0.98	0.12	0.56	0.72	0.69
El Centro	P-On	0.73	0.87	0.14	**1.23**	**2.85**	0.67	0.09	**1.61**	0.82
	P-Off	0.96	0.94	0.76	0.84	0.87	0.05	0.69	0.73	0.50
	Clip.	**1.25**	**1.23**	0.54	**1.26**	**1.61**	0.38	0.41	0.76	0.65
	Prop.	0.72	0.71	0.32	0.60	**1.08**	0.42	0.18	0.69	0.86
Rinaldi	P-On	0.94	0.96	0.50	0.97	**1.12**	0.29	0.27	0.83	0.86
	P-Off	**1.00**	**1.00**	0.95	0.99	**1.01**	0.05	0.84	0.86	0.34
	Clip.	**1.05**	**1.02**	0.60	0.97	**1.03**	0.27	0.38	0.72	0.77
	Prop.	0.91	0.90	0.73	0.85	0.86	0.13	0.49	0.56	0.71
Kobe	P-On	0.84	0.81	0.36	**1.19**	**2.33**	0.39	0.16	**1.14**	0.87
	P-Off	0.88	0.88	0.80	0.91	0.98	0.05	0.78	0.83	0.40
	Clip.	**1.05**	**1.03**	0.52	0.99	**1.63**	0.28	0.26	0.73	0.73
	Prop.	0.77	0.78	0.45	0.72	**1.05**	0.20	0.27	0.56	0.77
Jiji	P-On	0.83	0.82	0.65	0.86	0.92	0.17	0.42	0.82	0.70
	P-Off	0.96	0.96	0.93	0.96	0.96	0.03	0.85	0.91	0.25
	Clip.	0.84	0.84	0.65	0.86	0.87	0.17	0.46	0.72	0.64
	Prop.	0.94	0.95	0.84	0.97	0.99	0.06	0.68	0.82	0.48
Erzinkan	P-On	0.94	0.95	0.49	0.85	**1.21**	0.25	0.32	0.60	0.87
	P-Off	0.98	**1.00**	0.88	0.92	0.97	0.04	0.88	0.91	0.30
	Clip.	0.93	0.70	0.47	0.86	**1.23**	0.25	0.34	0.63	0.80
	Prop.	0.90	0.91	0.57	0.77	0.89	0.12	0.49	0.57	0.74

Table 5
Evaluation criteria for the proposed semi-active scheme compared with the clipped-optimal control algorithm in [3] and also with two limit cases: *passive off* and *passive on* (FP-*y* and FN-*x*).

Earthq.	Case	J_1	J_2	J_3	J_4	J_5	J_6	J_7	J_8	J_9
Newhall	P-On	0.83	0.93	0.51	**1.32**	**1.86**	0.34	0.33	**1.05**	0.89
	P-Off	0.90	0.92	0.87	**1.01**	**1.03**	0.04	0.81	0.87	0.40
	Clip.	0.88	0.92	0.55	**1.24**	**1.40**	0.30	0.42	0.84	0.79
	Prop.	0.79	0.82	0.62	**1.00**	**1.02**	0.17	0.47	0.70	0.78
Sylmar	P-On	0.79	0.78	0.68	0.80	**1.25**	0.25	0.46	0.67	0.85
	P-Off	0.98	0.98	0.99	0.97	0.98	0.03	0.86	0.85	0.34
	Clip.	0.80	0.79	0.74	0.79	0.92	0.24	0.51	0.61	0.81
	Prop.	0.85	0.83	0.89	0.80	0.87	0.09	0.62	0.61	0.68
El Centro	P-On	0.73	0.93	0.19	**2.18**	**3.46**	0.69	0.12	**1.99**	0.81
	P-Off	0.97	0.97	0.81	0.97	0.97	0.05	0.73	0.82	0.48
	Clip.	**1.26**	**1.25**	0.65	**1.41**	**1.93**	0.37	0.45	0.94	0.69
	Prop.	0.71	0.72	0.44	0.69	**1.06**	0.39	0.23	0.79	0.86
Rinaldi	P-On	0.88	0.93	0.53	0.93	**1.12**	0.28	0.24	0.58	0.87
	P-Off	0.93	0.98	0.89	**1.00**	**1.01**	0.05	0.83	0.82	0.34
	Clip.	0.98	**1.01**	0.62	0.99	**1.02**	0.27	0.30	0.47	0.78
	Prop.	0.84	0.81	0.63	0.90	0.90	0.13	0.40	0.42	0.72
Kobe	P-On	0.96	0.99	0.40	**1.30**	**2.24**	0.41	0.20	**1.44**	0.87
	P-Off	**1.01**	**1.01**	0.78	**1.00**	1.00	0.05	0.75	0.85	0.41
	Clip.	**1.15**	**1.20**	0.53	**1.33**	**1.47**	0.30	0.38	0.98	0.72
	Prop.	0.86	0.86	0.45	0.89	0.99	0.22	0.30	0.74	0.77
Jiji	P-On	0.74	0.74	0.63	0.75	0.77	0.17	0.40	0.74	0.70
	P-Off	0.97	0.97	0.92	0.97	0.97	0.03	0.86	0.89	0.26
	Clip.	0.74	0.73	0.63	0.73	0.80	0.17	0.46	0.61	0.64
	Prop.	0.91	0.91	0.81	0.91	0.92	0.05	0.69	0.76	0.48
Erzinkan	P-On	0.85	0.85	0.51	0.95	**1.13**	0.29	0.29	0.48	0.87
	P-Off	0.89	0.88	0.85	0.92	0.91	0.04	0.85	0.88	0.31
	Clip.	0.85	0.84	0.51	0.88	**1.16**	0.24	0.32	0.52	0.78
	Prop.	0.80	0.81	0.58	0.84	0.88	0.12	0.46	0.52	0.75

indices larger than 1 indicate that the response of the controlled structure is bigger than that of the uncontrolled structure. The performance indices larger than one in Tables 4 and 5 are highlighted in bold.

5.1. Performance indices

In this control strategy most of the response quantities are reduced substantially from the uncontrolled cases.

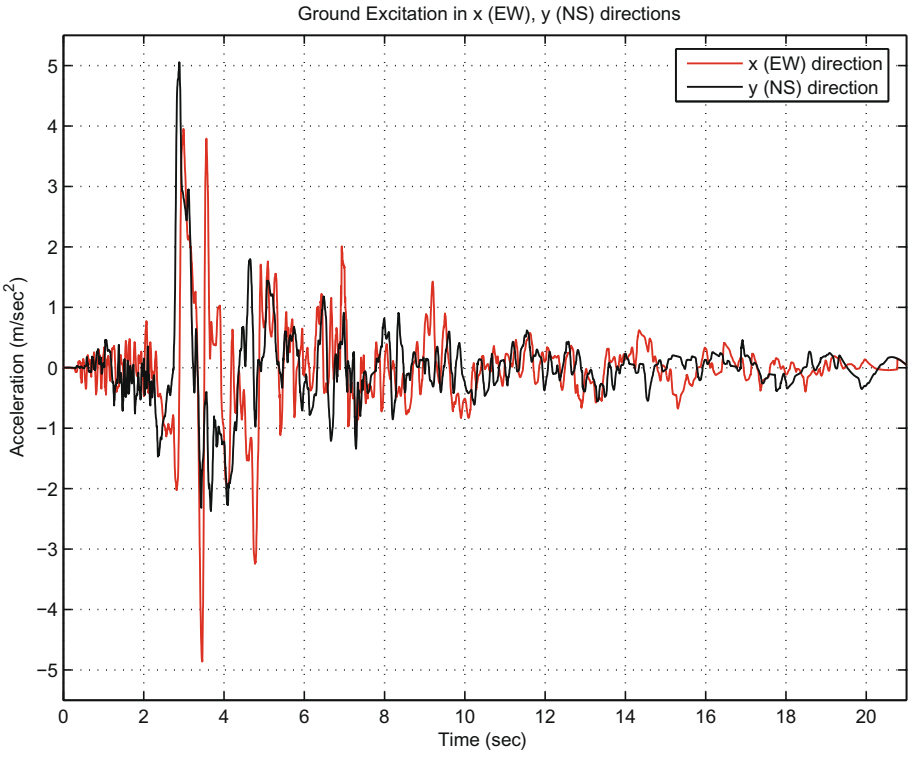

Fig. 13. 1992 Erzinkan earthquake, ground acceleration.

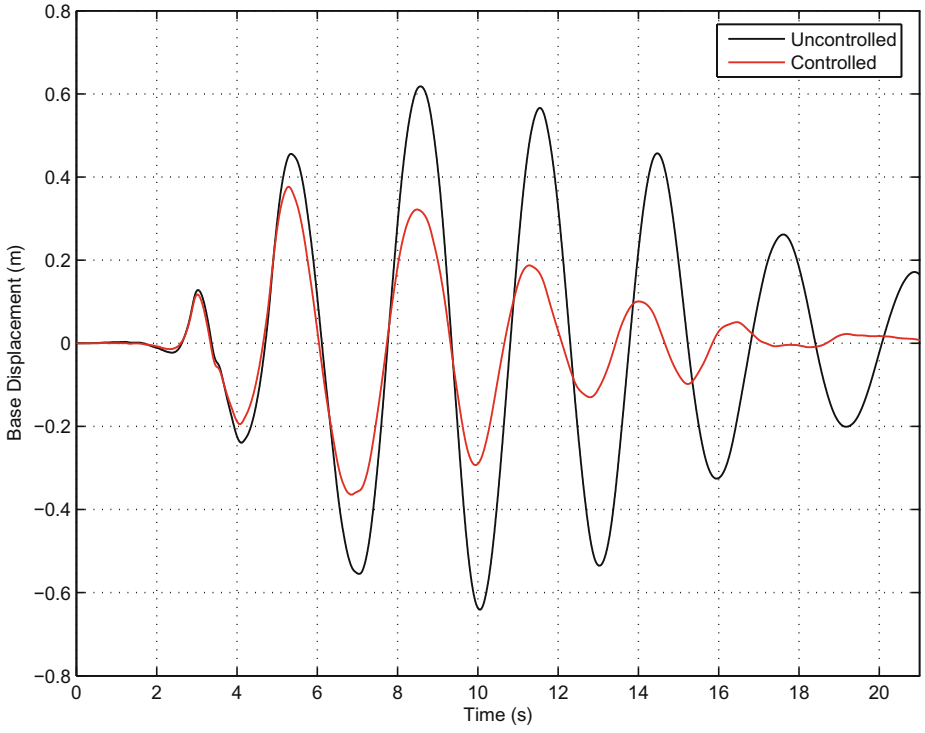

Fig. 14. Time history of response of the isolated building under Erzinkan excitation. Displacement of the center of the mass of the base in the *x*-direction for both the uncontrolled and the controlled situations.

The base and structural shears are reduced between 5 and 29% in all cases. The reduction in base displacement is between 11 and 68% also in all cases. Reductions in the interstorey drifts between 3 and 40% are achieved in a majority of earthquakes (except Newhall) when compared to the uncontrolled case. The floor accelerations are also reduced by 1–14% in a majority of earthquakes (except Newhall, El Centro and Kobe).

The benefit of the presented scheme is the reduction of base displacements (J_3) and shears (J_1, J_2) of up to 30 % without increase in drift (J_4) or accelerations (J_5). The reduction of the peak base

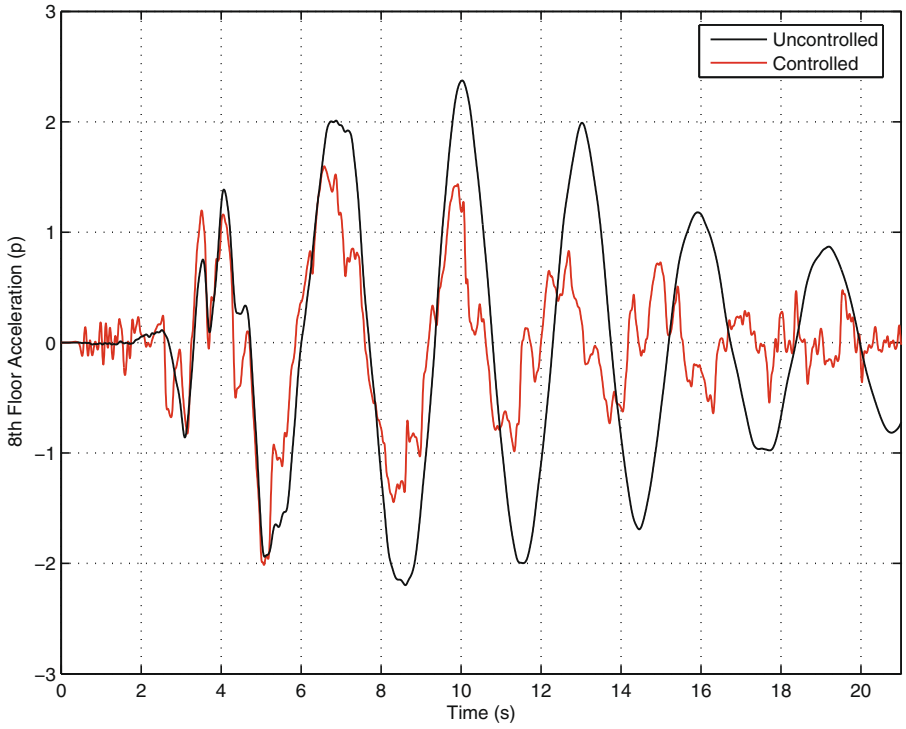

Fig. 15. Time history of response of the isolated building under Erzinkan excitation. Absolute acceleration of the eighth floor in the *x*-direction for both the uncontrolled and the controlled situations.

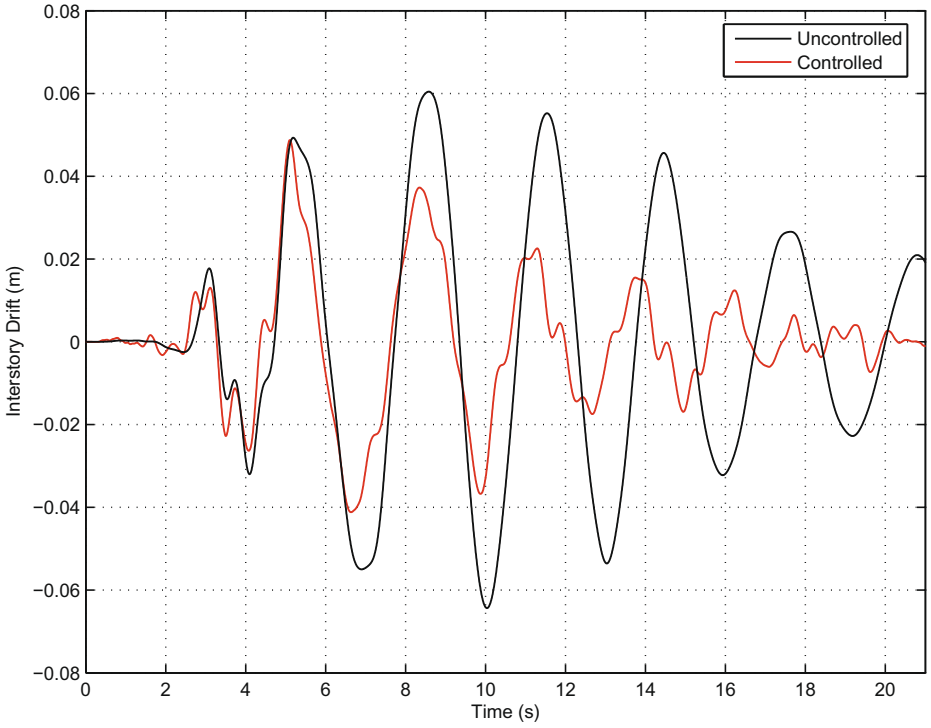

Fig. 16. Time history of the isolated building under Erzinkan excitation. Interstorey drift between the eighth floor and the seventh floor in the *x*-direction for both the uncontrolled and the controlled situations.

displacement J_3 of the base-isolated building is one of the most important criteria during strong earthquakes.

For the base-isolated buildings, superstructure drifts are reduced significantly compared to the corresponding fixed-buildings because of the isolation from the ground motion. Hence, a controller that reduces or does not increase the peak superstructure drift (J_4), while reducing the base displacement significantly (J_3), is desirable for practical applications. In this respect, the proposed semi-active controller performs well.

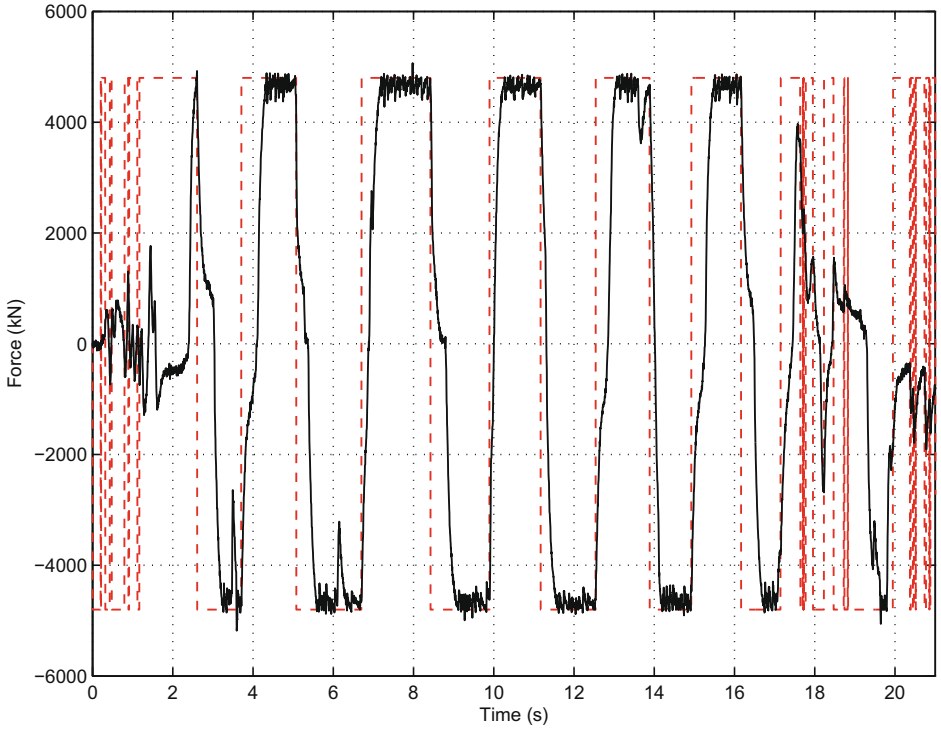

Fig. 17. Time histories of the desired control force (dashed) and the control force generated by the magnetorheological dampers (solid) in the *x*-direction under Erzinkan excitation.

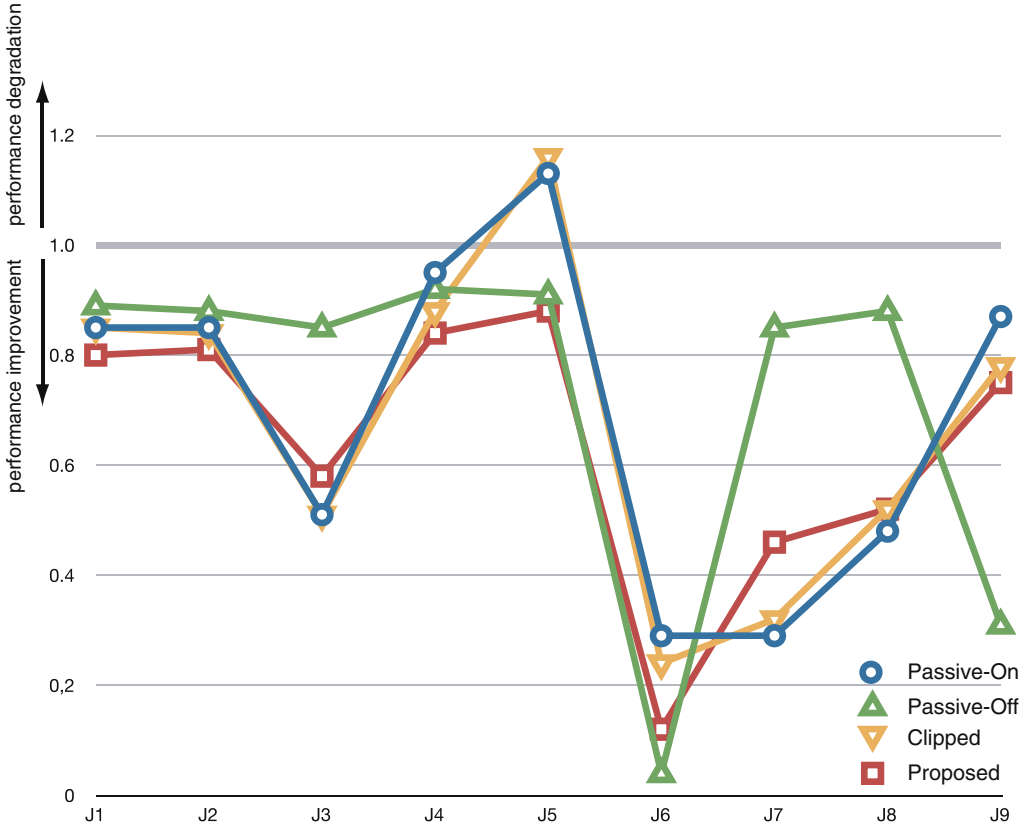

Fig. 18. Comparison of performance indices for various control systems (*passive on*, *passive off*, clipped-optimal and the proposed one) under Erzinkan excitation (FP-*y* and FN-*x*).

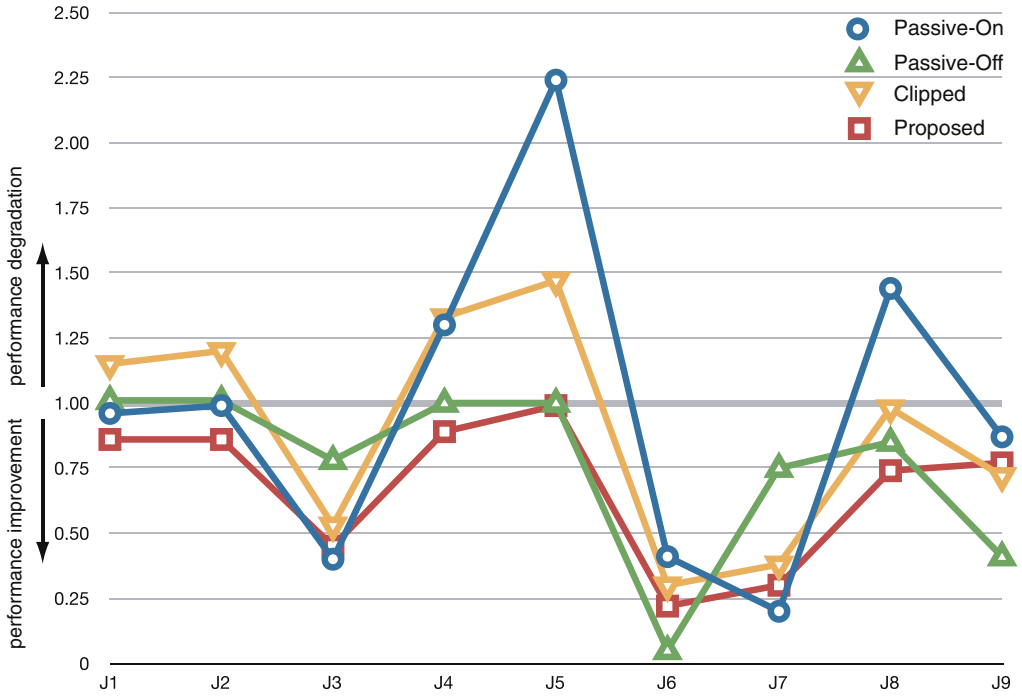

Fig. 19. Comparison of performance indices for various control systems (*passive on*, *passive off*, clipped-optimal and the proposed one) under Kobe excitation (FP-*y* and FN-*x*).

5.2. Time-history plots

Figs. 14–16 show the time-history plots of various response quantities for the uncontrolled building, and the building with the hierarchical semi-active control scheme using the Erzinkan FP-*x* and the FN-*y* earthquake. Fig. 13 shows the ground acceleration for this earthquake. More precisely, Fig. 14 presents the plots for the displacement of the center of the mass of the base in the *x*. The plotted quantities in Fig. 15 are the eighth floor absolute acceleration in the *x* direction for both the uncontrolled and the controlled situations. Finally, the interstorey drift between the eighth and the seventh floors in the *x* direction is depicted in Fig. 16. It is observed from these figures that the controlled response quantities can be effectively reduced compared with the uncontrolled case.

Fig. 17 shows the desired control force and the total damping force of the magnetorheological dampers in the *x* direction. It can be somehow observed that the total force generated by the MR dampers can closely follow the desired control force. Consequently, the implementation strategy presented in Section 3.4 seems reasonable.

5.3. Comparison

Fig. 18 shows that, as compared to the uncontrolled system – and for the Erzinkan excitation-, all of the isolation systems provide significant performance improvements in terms of reducing both peak and normed responses. The semi-active clipped optimal controller and the *passive on* performs better than the proposed hierarchical semi-active scheme with respect to the peak base displacement (J_3), but shows performance degradation with respect to the peak absolute floor acceleration (J_5). The results shown in Fig. 18 demonstrates that the proposed semi-active scheme produces improved performance beyond the *passive off* controlled system for indices $J_1 - J_5$. The same conclusions can be drawn from Fig. 19, where the performance indices under Kobe excitation are depicted. Overall, the proposed scheme produces simultaneous reduction in performance indices J_3,J_4 and J_5. Thus the goal of the hierarchical semi-active control, which is the simultaneous performance improvement of isolation system (J_3) and superstructure (J_4 and J_5) response, is achieved in the majority of cases. Therefore, the results provide validation of the effectiveness of the proposed algorithm.

6. Concluding remarks

A hierarchical semi-active control strategy has been presented in this paper, and has been applied to the control of the vibration response of a numerical three-dimensional benchmark building. A new inverse model of an MR damper has also been proposed to overcome the difficulty of commanding the MR damper to output the desired control force. This inverse model is based on (a) the extended normalized form of the Bouc–Wen model for MR dampers and (b) two simplifications on the parameters of the model. With respect to the implementation issues, a new practical method has been defined to compute the command voltage of each damper independently according to the desired control force: the management of these MR dampers is based on a hierarchical strategy. The whole method is simulated by considering a three-dimensional smart base-isolated benchmark building which is used by the structural control community as a state-of-the-art model for numerical experiments of seismic control attenuation. The performance indices demonstrate that the proposed semi-active method can effectively suppress structural vibration caused by earthquake loading and can provide a desirable effect of structural performance.

Appendix A. Evaluation criteria

The following nine evaluation criteria are defined for the benchmark problem based on both maximum and RMS responses of the building. In the following discussion, the term *uncontrolled* refers to the isolation system with no supplemental control devices.

These evaluation criteria are reproduced here to assist the reader in comprehending this paper.

1. Peak base shear (isolation level) in the controlled structure normalized by the corresponding shear in the uncontrolled structure

$$J_1(q) = \frac{\max_t \|V_0(t,q)\|}{\max_t \|\widehat{V}_0(t,q)\|}$$

2. Peak structure shear (at first storey level) in the controlled structure normalized by the corresponding shear in the uncontrolled structure

$$J_2(q) = \frac{\max_t \|V_1(t,q)\|}{\max_t \|\widehat{V}_1(t,q)\|}$$

3. Peak base displacement or isolator deformation in the controlled structure normalized by the corresponding displacement in the uncontrolled structure

$$J_3(q) = \frac{\max_{t,i} \|d_i(t,q)\|}{\max_{t,i} \|\hat{d}_i(t,q)\|}$$

4. Peak interstorey drift in the controlled structure normalized by the corresponding interstorey in the uncontrolled structure

$$J_4(q) = \frac{\max_{t,f} \|d_f(t,q)\|}{\max_{t,f} \|\hat{d}_f(t,q)\|}$$

5. Peak absolute floor acceleration in the controlled structure normalized by the corresponding acceleration in the uncontrolled structure

$$J_5(q) = \frac{\max_{t,f} \|a_f(t,q)\|}{\max_{t,f} \|\hat{a}_f(t,q)\|}$$

6. Peak force generated by all control devices normalized by the peak base shear in the controlled structure

$$J_6(q) = \frac{\max_t \|\sum_k F_k(t,q)\|}{\max_t \|V_0(t,q)\|}$$

7. RMS base displacement in the controlled structure normalized by the corresponding RMS base displacement in the uncontrolled structure

$$J_7(q) = \frac{\max_i \|\sigma_d(t,q)\|}{\max_i \|\sigma_{\hat{d}}(t,q)\|}$$

8. RMS absolute floor acceleration in the controlled structure normalized by the corresponding RMS acceleration in the uncontrolled structure

$$J_8(q) = \frac{\max_f \|\sigma_a(t,q)\|}{\max_f \|\sigma_{\hat{a}}(t,q)\|}$$

9. Total energy absorbed by all control devices normalized by energy input into the controlled structure

$$J_9(q) = \frac{\sum_k \left[\int_0^{T_q} F_k(t,q)\, v_k(t,q)\, dt\right]}{\int_0^{T_q} \langle V_0(t,q)\dot{U}_g(t,q)\rangle dt}$$

where, i = isolator number,$1,\ldots,N_i$ ($N_i = 8$); k = device number, $1,\ldots,N_d$; f = floor number,$1,\ldots,N_f$; q = earthquake number, $1,\ldots,7$; t = time,$0 \leqslant t \leqslant T_q$; $\langle\cdot\rangle$ = inner product;$\|\cdot\|$ = vector magnitude incorporating NS and EW components.

These nine performance criteria are in-line with the information typically used to design and analyze typical civil structures [11].

References

[1] Bahar A, Pozo F, Acho L, Rodellar J, Barbat A. Parameter identification of large-scale magnetorheological dampers in a benchmark building. Computers and Structures 2010;88:198–206.

[2] Dominguez A, Sedaghati R, Stiharu I. Modeling and application of MR dampers in semi-adaptive structures. Computers and Structures 2008;86(3–5):407–15.

[3] Dyke SJ, Spencer Jr BF, Sain MK, Carlson JD. Modeling and control of magnetorheological dampers for seismic response reduction. Smart Materials and Structures 1996;5(5):565–75.

[4] Gu ZQ, Oyadiji SO. Application of MR damper in structural control using ANFIS method. Computers and Structures 2008;86(3–5):427–36.

[5] Ikhouane F, Rodellar J. Systems with Hysteresis: Analysis. Identification and Control Using the Bouc–Wen Model. John Wiley and Sons, Inc.; 2007.

[6] Ikhouane F, Mañosa V, Rodellar J. Adaptive control of a hysteretic structural system. Automatica 2005;41(2):225–31.

[7] Jung HJ, Choi KM, Spencer Jr BF, Lee IW. Application of some semi-active control algorithms to a smart base-isolated building employing MR dampers. Structural Control and Health Monitoring 2006;13(2–3):693–704.

[8] Li H, Ou J. A design approach for semi-active and smart base-isolated buildings. Structural Control and Health Monitoring 2006;13(2–3):660–81.

[9] Luo N, Rodellar J, Vehí J, De la Sen M. Composite semiactive control of a class of seismically excited structures. Journal of the Franklin Institute 2001;338(2–3):225–40.

[10] Naeim F, Kelly JM. Design of Seismic Isolated Structures: From Theory to Practice. John Wiley and Sons; 1999.

[11] Narasimhan S, Nagarajaiah S, Johnson EA, Gavin HP. Smart base-isolated benchmark building. Part I: problem definition. Structural Control and Health Monitoring 2006;13(2–3):573–88.

[12] Pozo F, Acho L, Rodríguez A, Pujol G. Nonlinear modeling of hysteretic systems with double hysteretic loops using position and acceleration information. Nonlinear Dynamics 2009;57(1–2):1–12. doi:10.1007/s11071-008-9414-7.

[13] Pozo F, Montserrat PM, Rodellar J, Acho L. Robust active control of hysteretic base-isolated structures: application to the benchmark smart base-isolated building. Structural Control and Health Monitoring 2008;15(5):720–36.

[14] Ramallo JC, Johnson EA, Spencer BF. "Smart" base isolation systems. Journal of Engineering Mechanics 2002;128(10):1088–99.

[15] Rodríguez A, Ikhouane F, Rodellar J, Luo N. Modeling and identification of a small-scale magnetorheological damper. Journal of Intelligent Material Systems and Structures, doi: 10.1177/1045389X08098440.

[16] Rodríguez A, Iwata N, Ikhouane F, Rodellar J. Model identification of a large-scale magnetorheological fluid damper. Smart Materials and Structures 2009;18(1). doi:10.1088/0964-1726/18/1/015010.

[17] Skinner RI, Robinson WH, McVerry GH. An Introduction to Base Isolation. John Wiley and Sons; 1992.

[18] Wen YK. Method of random vibration of hysteretic systems. Journal of Engineering Mechanics 1976;102(2):249–63.

[19] Yoshida O, Dyke SJ. Seismic control of a nonlinear benchmark building using smart dampers. Journal of Engineering Mechanics 2004;130(4):386–92.